Full Length Article

Breakdown of the correlation between oxidation states and core electron binding energies at the sub-nanoscale

Federico Loi [a], Monica Pozzo [b], Luca Sbuelz [a], Luca Bignardi [a], Paolo Lacovig [c], Ezequiel Tosi [c], Silvano Lizzit [c], Aras Kartouzian [d], Ulrich Heiz [d], Rosanna Larciprete [e], Dario Alfè [b,f], Alessandro Baraldi [a,c,*]

[a] Department of Physics, University of Trieste, via Valerio 2, Trieste 34127, Italy
[b] Department of Earth Sciences and London Centre for Nanotechnology, University College London, Gower Street, London WC1E 6BT, UK
[c] Elettra Sincrotrone Trieste, Str. St. 14 km 163.5 in AREA Science Part, Basovizza, Trieste 34149, Italy
[d] Department of Chemistry, Technical University of Munich, Lichtenbergstrasse 4, Garching 85748, Germany
[e] CNR-Institute for Complex Systems, via dei Taurini 19, Roma 00185, Italy
[f] Dipartimento di Fisica Ettore Pancini, Università di Napoli Federico II, Monte S. Angelo, Napoli 80126, Italy

ARTICLE INFO

ABSTRACT

X-ray photoelectron spectroscopy is a powerful analytical tool to fingerprint the atomic oxidation state. However, the well-established trend that is found for bulk, ultra-thin films and surface oxides, which is usually characterized by an incremental binding energy shift upon increasing oxidation state, may not apply at the sub-nanoscale where reduced dimensionality and quantum size effects play a relevant role. Here we investigate through a combined experimental and theoretical approach the oxidation of size-selected Ag_7 and Ag_{11} clusters supported on graphene, revealing an anomalous Ag $3d_{5/2}$ core level shift trend upon increasing O coverage. We show that the negative core level shift trend typical of Ag reverts back in the case of the highest Ag(III) oxidation state, an effect that is due to the peculiar electronic structure of Ag nano-oxides. Our results highlight the great care needed to extend at the zero-dimensional scale the knowledge acquired for the spectral interpretation of 3D and 2D materials.

1. Introduction

The concept of oxidation state or oxidation number constitutes an essen- tial trait of a material, intimately connected with its specific electronic struc- ture and the nature of chemical bonds [1]. Besides the widespread application of theoretical approaches, ranging from the bond valence sum method [2] to density functional theory calculations [3] and the most recent applications of the state-of-the-art machine learning [4], X-ray photoelectron spectroscopy (XPS) has proven to be an extremely powerful experimental technique to study this aspect of matter since the pioneering work by Kai Siegbahn and co-workers [5]. The composition and chemical nature of solid surfaces has been deeply investigated thanks to the ability to distinguish spectral com- ponents separated even by only a few hundred meV, allowing to create an extensive XPS database of the oxidation state of many elements of the periodic table. Copper provides a textbook example of this, since the 1 *s* core level shifts by + 4.4 eV going from the metallic to the oxide phase

[6]. The capability to identify exactly the oxidation state in copper compounds is nowadays of paramount importance for a wide set of chemical processes [7,8,9,10].

For heavier elements, such as tantalum and tungsten, the observation of discrete, evenly spaced $4f_{7/2}$ core level shifts (CLS) brought to reveal a large number of possible non-equivalent oxidation states [11]. The nature behind these shifts relies on the correlation of the exact peak position of the core level lines to the oxidation level of the emitting atom and to the electric field generated by adjacent atoms. In general, when the emitting atom is bound with a more electronegative ligand such as oxygen, it undergoes a withdrawal of electrons, making it harder to photoexcite its core electrons, which thus have a higher binding energy (BE). Ag represents and exception to this rule, as atoms with a higher oxidation state show lower BEs [12,13]. This applies also to the oxidation of ultra-thin Ag films, which potentially allow to achieve higher oxidation conditions compared to bulk foils. In this case, the BE of the Ag $3d_{5/2}$ core level assigned to Ag(0), Ag(I) and Ag(III) oxidation states was

---

respectively 368.24, 367.30 and 366.80 eV [14]. Similarly, for Ag(1 1 1) the absolute value of the CLS increases linearly with the number of oxygen neighbors as for a wide range of transition metals [15–17], but with a negative trend. Calculated Ag $3d_{5/2}$ CLS for the p(4 × 4) configuration of the oxidized Ag(1 1 1) surface are found to be −0.28, −0.60 and −0.81 eV when Ag forms a bond with one, two and three oxygen atoms respectively [18]. The same behavior was found also in the case of Ag(1 0 0) with a number of O neighbors up to four [19], thus suggesting that the trend has a general validity for Ag surfaces. The motivations behind this trend is attributed to the peculiar electronic band structure of Ag. Calculations on the valence electronic structure and for the initial state effect contributions to the CLS of a Ag(1 1 1) surface at different O coverage showed that the onsite Ag core potential is almost not affected by oxidation, despite a clear metal-to-oxygen charge transfer. For this reason, the calculated CLS was attributed to final state effects arising from the inefficient screening of bonding s states [18,20]. The recent observation that the oxidation of a size-selected Ag$_{11}$ cluster leads to a bulk-like hybrid structure composed of both Ag(III) and Ag(I) ions [21], prompted us to investigate the CLS anomaly of Ag oxides at the sub-nanoscale. In this work we studied the oxidation of Ag$_7$ and Ag$_{11}$ clusters supported on graphene by means of high-resolution XPS and *ab initio* DFT calculations. We found that the Ag $3d_{5/2}$ CLS of the atoms in the clusters follows the negative trend typical of Ag until the number of Ag-O bonds (N_B) is below 3. When moving to $N_B = 4$, which corresponds to Ag(III) ions [21], the CLS suddenly moves back towards Ag(0). The final result of this trend is that Ag(III) ions in oxidized Ag$_7$ and Ag$_{11}$ clusters show a Ag $3d_{5/2}$ BE higher than Ag(I). We interpret this effect as a result of the direct response of the d-band center ϵ_d of the Ag atoms in the clusters to the increasing number of Ag-O bonds which enhances the initial state contribution to the overall CLS. This is a striking difference compared to bulk, ultra-thin films and surface Ag oxides which indicates that the well-established trends found in bulk matter and on solid surfaces might differ greatly for atomic clusters because of their reduced dimensionality and unique electronic properties.

2. Methods

2.1. Sample preparation

A Ru(0001) single crystal was cleaned by repeated cycles of Ar$^+$ sputtering and annealing in O$_2$ atmosphere between 600 and 1000 K. The residual oxygen was removed by a final flash annealing up to 1500 K. Graphene was grown by thermal decomposition of ethylene (C$_2$H$_4$) at 1100 K. The precursor pressure was initially set to 5×10^{-9} mbar and successively increased in steps up to 5×10^{-8} mbar to ensure that entire surface was covered by graphene. The resulting graphene layer showed the typical low energy electron diffraction (LEED) pattern with sharp moiré spots reported in Figure S4 [22].

2.2. Deposition of Ag nanoclusters

Ag$_7^+$ and Ag$_{11}^+$ positive clusters were produced using the cluster source ENAC. This cluster source is based on the laser ablation of a metal target. The mass selection of clusters is performed with a quadrupole mass analyzer and a mass scan reported in Supplementary Information. A more detailed description of the source is reported elsewhere [23,24]. The clusters were deposited on graphene/Ru(0001) (Gr/Ru), on which they are electrically neutralized. The amount of clusters reaching the Gr/Ru surface was mon- itored by reading directly the current on the sample, on which we applied a positive voltage to reduce the kinetic energy E_k of the clusters to ensure the soft landing conditions (E_k less than 1 eV/atom) [25]. To avoid Ag cluster sintering, the cluster density was below 9×10^{-3} cluster/nm^2 and the tem- perature of the sample was kept at 20 K during the deposition, reaction, and measurements.

2.3. High-Resolution X-ray photoelectron spectroscopy

High-resolution X-ray photoelectron spectroscopy (HR-XPS) mea- sure- ments were performed in-situ at the SuperESCA beamline at Elettra-Sincrotrone Trieste, Italy. The photoemission spectra were collected by means of a Phoibos 150 mm mean radius hemispherical electron energy analyzer from SPECS, equipped with a delay line de- tector developed in-house. The overall energy resolution was better than 50 meV for the photon energies and parameters employed. The binding energy scale was calibrated to the Fermi level position of the metallic substrate. The XPS spectra were acquired by tuning the photon energy to have a photoelectron kinetic energy of about 100 eV, to enhance surface sensitivity. For each spectrum, the photoemission intensity was normalized to the photon flux and the BE scale was aligned to the Fermi level of the Ru(0001) substrate. Core level spectra were analyzed using a Doniach-Sunjic [26] line profile for each spectral component, combined with a Gaussian distribution to account for the experimental, phonon and inhomogeneous broadening. The background was modeled with a second-degree polynomial curve for every Ag $3d_{5/2}$ spectrum.

2.4. Theoretical methods

The calculations have been performed using density functional the- ory (DFT) as implemented in the VASP code [27]. The systems were described with a slab with 4 layers of Ru in a 12 × 12 hexagonal supercell and a layer of 13 × 13 unit cell of graphene placed on top with an overall number of 914 atoms, excluding the Ag$_{11}$ and Ag$_7$ cluster. The Ag cluster was placed on the valley of the corrugated graphene layer, with his center on a fcc site, where the stronger interaction with the Ru (0001) substrate increases its stability [28]. The bottom two layers of Ru were kept frozen at their bulk geometry, with a lattice parameter of 2.724 Å, and the rest of the system was fully relaxed using the rev-vdw-DF2 functional [29] until the largest residual force was less than 0.015 eV/Å. We employed the projector augmented method (PAW)[30] using PBE[31] potentials. The plane wave cutoff was set to 400 eV, and the relaxations were performed by sampling the Brillouin zone using the Γ point only. To obtain the partial density of states (PDOS) we have per- formed single point DFT calculations, using geometries obtained with the rev-vdw-DF2 functional. Core-electron BEs have been estimated in the final-state approximation, therefore including also final state effects due to core–hole screening.

3. Results and discussion

3.1. Deposition of Ag nanoclusters on graphene/Ru(0001)

Positive Ag$_7^+$ and Ag$_{11}^+$ clusters were generated using the cluster source ENAC, whose detailed description is reported elsewhere [23,24]. The clus- ters were deposited under soft landing conditions on gra- phene/Ru(0001) (Gr/Ru), on which they are electronically neutralized. The Gr monolayer supported on Ru was chosen for its low interaction with Ag [32] and for its corrugated morphology [33]. The weak inter- action is required to reduce the modifications of the properties of the unsupported size-selected clus- ters, while the corrugation decreases the mobility of the atomic aggregates on the surface and prevents their coalescence as proved for several systems [34,35,36,21]. To further reduce the probability of sintering, the cluster density on Gr/Ru was kept below 9×10^{-3} cluster/nm^2 (about one cluster every 3000 carbon atoms). For the same reasons, the sample temperature during deposi- tion, reaction and measurements was always maintained at 20 K. These conditions prevent the occurrence of oxidative dispersion of clusters, a mechanism that has been found in the case of Ag clusters after oxygen exposure in the mbar pressure range and at temperature of 700 K [37]. We focused our interest on two different clusters: Ag$_{11}$ for its ability to reach a bulk-like hybrid structure composed of atoms with different oxidation states, namely 1+ and 3+ [21], and Ag$_7$, the largest planar Ag

cluster according to our DFT calculations, with the aim to understand if the core electron binding energy behaviour is affected by the cluster morphology. It is interesting to note that even Au_7 assumes the same planar hexagonal configuration on Al_2O_3 surfaces, according to DFT calculations [38] The minimum energy configurations of the positively charged clusters in the gas-phase are shown in Supplementary Information.

3.2. High-resolution XPS of pristine Ag clusters

High-resolution XPS measurements were performed *in situ* at the SuperESCA beamline of the Elettra synchrotron radiation facility, Trieste. The Ag $3d_{5/2}$ spectra were acquired in normal emission and with a photon energy of 470 eV, with a total energy resolution better than 50 meV. Fig. 1a shows a comparison between the Ag $3d_{5/2}$ core level of an Ag(1 1 1) single crystal surface, an Ag polycrystalline slab and the two size selected clusters. The Ag(1 1 1) surface was fitted with two components separated by 150 meV, one associated to bulk atoms (368.20 eV) and the second to surface atoms (368.05 eV) [24]. The polyscristalline and the cluster spectra were fitted using a single component located at 368.17 eV for the slab, 368.17 eV for Ag_{11} and 368.24 eV for Ag_7. The Ag $3d_{5/2}$ binding energies of the clusters are rather similar to bulk and polycrystalline sample, in agreement with previous results on Ag sieze-selected clusters [39] and nanoparticles deposited on highly oriented pyrolytic graphite (HOPG) [40]. Our fitting analysis indicates that Ag_7 has a BE 70 meV higher than Ag_{11}, following a trend similar to that found for Pd size-selected clusters [41]. This trend was confirmed by DFT calculations that were carried out placing isolated Ag_7 and Ag_{11} in a Gr/Ru moiré cell supported by 4 Ru layers. In Fig. 1b and 1c we show zoomed side and top views on the resulting relaxed structures. The complete unit cell is shown in Supplementary Information. While the structure of adsorbed Ag_{11} is almost preserved with respect to the the one found for the corresponding gas-phase ion, Ag_7 show a slightly modified conformation, with silver atoms moving out from the planar configuration, an indication that the interaction with the carbon network is not completely negligible [42].

It is worth comparing the full width at half maximum (FWHM) of the Ag $3d_{5/2}$ core level measured for the clusters with that one observed for our reference sample, which appears to be narrower. Such outcome is not totally unexpected and it is determined by a concurrence of factors. First of all, it is important to stress that the broadening observed for clusters results from the different local configurations and different co-ordination numbers of the non-equivalent atoms. An important parameter to consider in such case is the effective coordination, which accounts for the presence of the first-neighbor atoms, but also for the local modifications of the interatomic distances. Second, it cannot be neglected that different non-equivalent atoms undergo slightly different screening effects. Last, it is not possible to com- pletely rule out the vibrational effects, intrinsic to the photoemission process, which contribute to the line broadening even if the sample temperature is very low. We are indeed studying systems which are not in their bulk form and to which we can associate a set of vibrational frequencies producing a general broadening of the photoemission peak. Such phenomenon has been already well documented for core levels of molecules adsorbed on surfaces [43]. Earlier work reporting photoemission data on small size-selected Ag clusters deposited on sputter damaged HOPG have already pointed out that the core levels are considerably larger in terms of FHWM than metallic surfaces. For the latter the lower surface-to-volume ratio will indeed lead to a less heterogeneous chemical environment of Ag atoms with respect to the cluster case and, therefore, to the
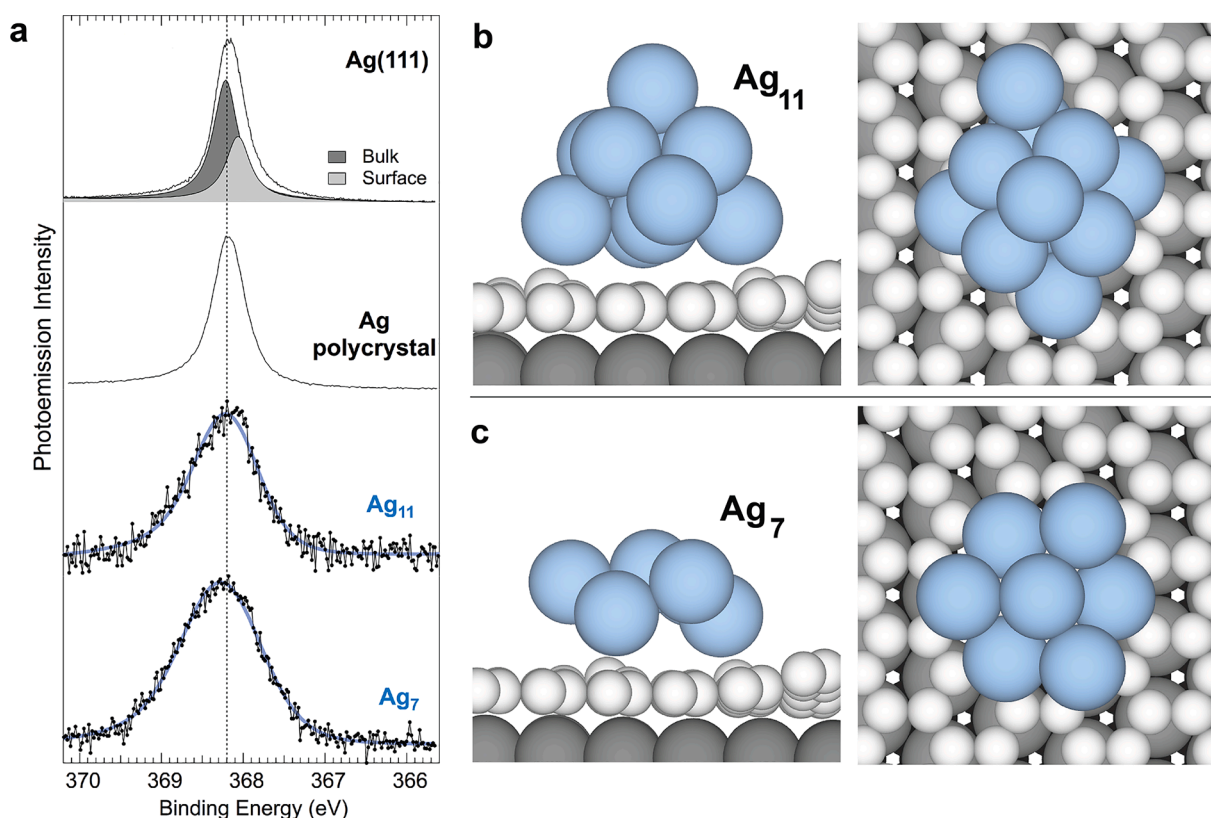

Fig. 1. (a) Ag $3d_{5/2}$ core level spectra of Ag(1 1 1) (with surface and bulk component displayed in light and dark gray, respectively), Ag polycrystal and of the size-selected Ag_7 and Ag_{11} clusters supported on Gr/Ru. The blue lines represents the fitting curves resulting from the data analysis. Top and side views of the DFT calculated relaxed structures of the Ag clusters: (b) Ag_{11} and (c) Ag_7. White balls represent C atoms, gray and black balls represent first layer and bulk Ru atoms, respectively, red and light blue stand for Ag. (For interpretation of the references to colour in this figure legend, the reader is referred to the web version of this article.)

narrowing of the line-shape [39]. In particular, the FWHM increases inversely with the cluster size [44], in good agreement with our experimental results, where the Gaussian parameter obtained from the spectral analysis is 0.97 eV for Ag_7 and 0.73 eV for Ag_{11}.

3.3. High resolution XPS and DFT calculations: Core level shift anomaly in the oxidized clusters

The oxidization of the clusters was achieved by using a photon-induced dissociation process, where atomic oxygen is obtained by irradiation of ph- ysisorbed O_2 with soft X-rays at T = 20 K [21,45]. Fig. 2 shows that an exposure to 0.1 L (low oxidation), where $1L = 1 \times 10^{-6}$ torr × 1 s, leads to a CLS towards lower binding energies for both Ag_{11} and Ag_7. The CLS further increases upon a second exposure to 0.5 L (high oxidation). This behavior reminds us the trend observed for the oxidation of (1 1 1) and (1 0 0) single crystal silver surfaces, where, as reported above, the CLS is attributed to final state effects and increases linearly with N_B [18,19]. For larger oxygen exposures and prolonged photon irradiation, the Ag $3d_{5/2}$ spectra of the Ag_7 and Ag_{11} clusters did not change.

To understand how the measured data are related to the Ag oxidation at the atomic scale, we employed DFT to calculate the minimum energy config- urations and the electronic structural modifications induced by an increasing O density on the clusters. To compare the effects of oxidation of the clusters with the oxidation of Ag surfaces and to understand if the trend observed in the latter case is preserved also at the sub-nanoscale, we calculated the oxygen induced CLS in the final-state approximation on each Ag atom of the clusters at different O coverage. Ag $3d_{5/2}$ core electron binding energies reported in Fig. 2c-d correspond to 195 non-equivalent configurations that have been calculated and for a total of 21 $Ag_{11}O_m$ and Ag_7O_m oxidized clusters, with $m = 0–10,12$ and $m = 0–8$, respectively. For both sys- tems we reached a O:Ag ratio slightly larger than 1. The minimum energy relaxed structures are reported in Supplementary Information. We have as well investigated the dependence of the distribution of binding energies on the cluster configuration on the graphene substrate, both for the pristine Ag_{11} and for $Ag_{11}O_2$ clusters with the two O atoms positioned in different adsorption sites. In both cases, the differences observed are much smaller than the standard deviation calculated for the binding energy distributions. More details about this feature are reported in Supplementary Information. The calculations show that the Ag $3d_{5/2}$ spectral weight moves, for both clusters, towards lower binding energies for increasing O density, in good agreement with our experimental findings. The broad distribution of the calculated core electron binding energy is in excellent agreement with the experimental findings which show that the width of cluster spectra is considerably larger than the one
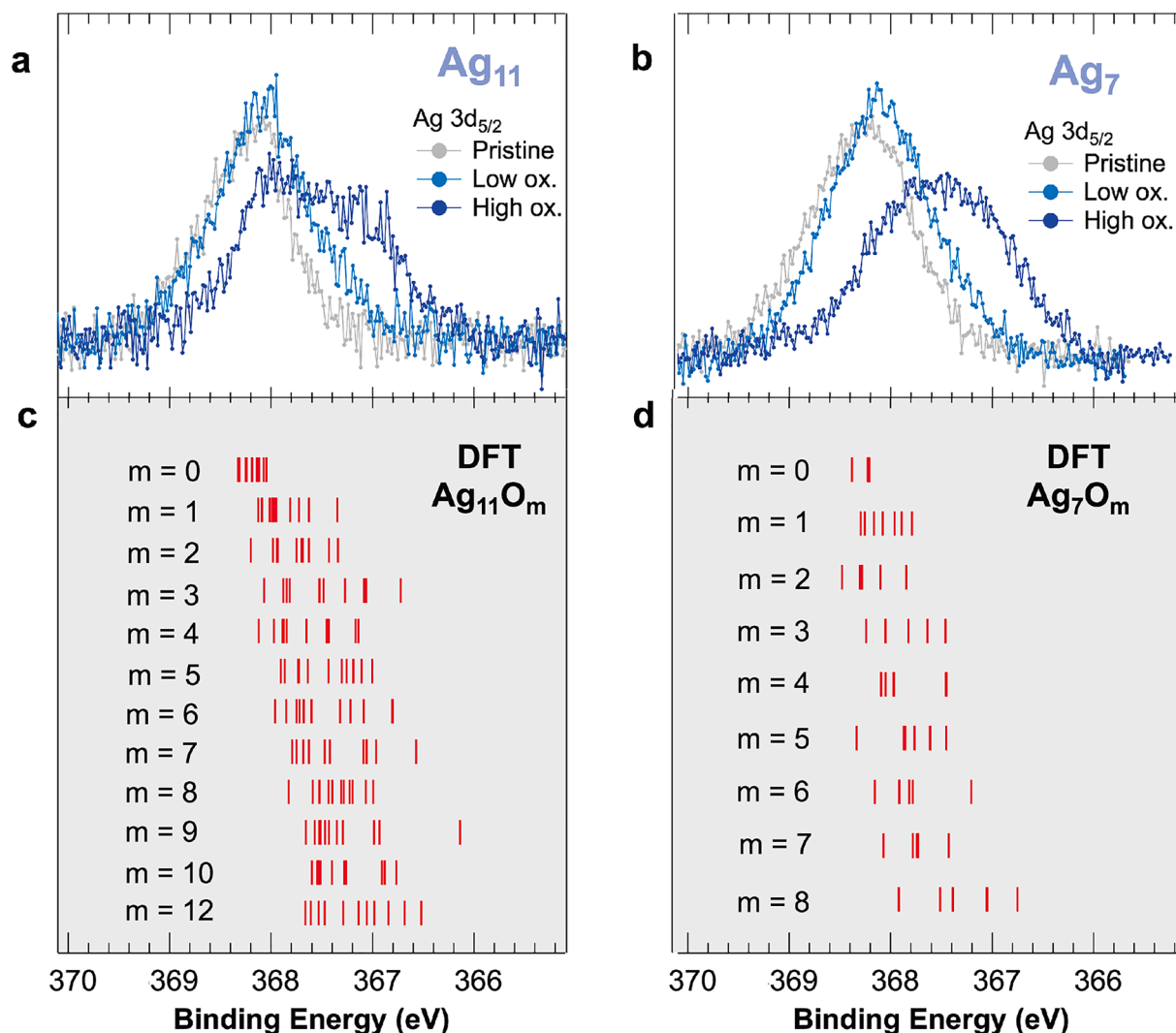

Fig. 2. (a) Ag $3d_{5/2}$ core level spectra following the oxidation of the Ag_{11} and (b) Ag_7 size-selected cluster on Gr/Ru. We report the clean (light gray), mild (0.1 L of O_2, light blu) and highly (0.5 L of O_2, blu) oxidized clusters. (c) DFT calculated $3d_{5/2}$ core level binding energy for each Ag atom composing the oxidized $Ag_{11}O_m$ supported clusters, with $m = 0–10$ and 12. **d** Similar calculations for the atoms of the Ag_7O_m supported clusters, with $m = 0–8$.

obtained for the Ag(1 1 1) single cyrstal or the sputtered/annealed polycrystal. The possibility of performing *ab initio* calculations for an increasing oxygen density in steps of a single oxygen atom was of paramount importance to obtain the trend of Ag $3d_{5/2}$ core levels vs N_B, i.e., the number of oxygen bonds (Fig. 3a). In the present work, we define N_B as the number of oxygen atoms that are bound to a given Ag atom with a O – Ag bond length below the threshold of 2.30 Å. This

value arises from the O – Ag distance which typically ranges from 1.90 Å to 2.30 Å, for the bulk systems that we investigated (AgO, Ag_2O_3, etc), for the oxidized Ag_{11} and Ag_7 nanoclusters, as well for oxidized silver surfaces [19]. The CLSs are expressed using the bulk Ag $3d_{5/2}$ BE (368.20 eV) as reference.

Fig. 3a indicates that the amplitude of the negative CLS in the clusters increases linearly for $N_B = 0$–2, but the trend surprisingly breaks-
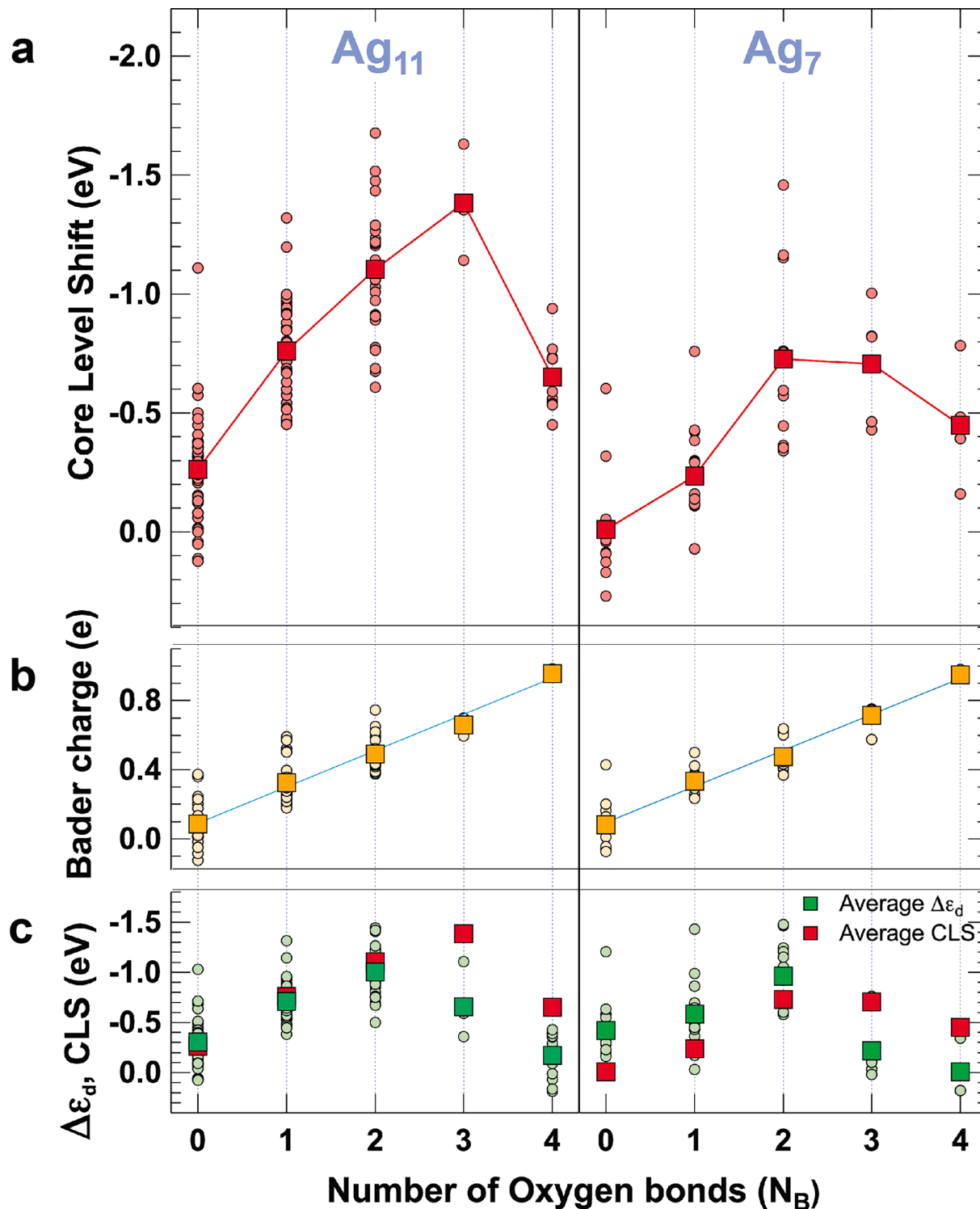

Fig. 3. Electronic properties of the oxidized clusters vs N_B. (a) Calculated Ag $3d_{5/2}$ CLSs, (b) Bader charge and (c) $\Delta\epsilon_d$ for the oxidized Ag_{11} -left panel- and Ag_7 clusters -right panel- as a function of the number N_B of the Ag-O bonds per Ag atom. Filled circles are the full set of calculations while square markers represent the average valued for each N_B.

down for larger values. Specifically, for Ag$_7$ the trend is linear (as one can see by fitting the whole set of data points) in the range N_B = 0–2 with a slope of −0.34 eV/N_B, while for Ag$_{11}$ the linear trend continues up to N_B = 3 with a steeper slope of −0.41 eV/N_B. Such values are similar to those found for a Ag(1 0 0) surface up to N_B = 4, where the CLS increases by −0.29 eV/N_B [19]. On the contrary, when moving to N_B = 4, the Ag $3d_{5/2}$ CLS in the clusters decreases. For Ag$_7$, it goes from −0.65 eV for N_B = 3 to −0.45 eV, while the difference is even more pronounced for Ag$_{11}$, where the CLS decreases from −1.40 eV for N_B = 3 to −0.65 eV for N_B = 4.

In a recent publication [21], we have demonstrated that Ag atoms in the clusters with N_B = 2 and N_B = 4 possessing the typical planar morphology observed in AgO bulk oxide correspond to d^{10} Ag(I) and d^8 Ag(III) ions, respectively. Hence, we can conclude observing the trends in Fig. 3a that the CLS for Ag(III) ions is lower than for Ag(I). This is a striking difference with respect to Ag bulk oxides and thin films [14], where the BEs are ordered as Ag(0) > Ag(I) > Ag(III).

To explain the origin of this anomalous trend of the Ag oxidation state vs CLS, we performed (i) a Bader charge analysis [21,18,46] (see Fig. 3b) and (ii) calculated the shift of the Ag d-band center ϵ_d ($\Delta\epsilon_d$) of the atoms of the oxidized clusters (see Fig. 3c), mimicking the approach used to study the oxidation of Ag(1 1 1), which lead to the attribution of the negative CLS to the dominant final state contribution [18]. The trend of the calculated Bader charge vs N_B for both Ag clusters, which is reported in Fig. 3b, is still linear even for N_B = 4 (linear correlation coefficient = 0.97 ± 0.02 and slope 0.21 e/bond). No anomalies can be appreciated in the whole range. This out- come mirrors indeed entirely the results of the calculations reported for the Ag(1 1 1) surface [18], for which a very similar slope of the Bader charge (0.22 e/bond) can be extrapolated. This trend clearly indicates that the oxidation state of the Ag atoms in both Ag$_{11}$ and Ag$_7$ clusters increases linearly with N_B as it happens for the oxidation of the Ag(1 1 1) surface. Therefore, the non-monotonic trend of the CLS is not directly linked to anomalous charge transfer effects between oxygen and Ag atoms upon increasing N_B.

The second part of the analysis we performed was focused on the study of the trend of $\Delta\epsilon_d$ (expressed with respect to the bulk Ag value which we calculated to be ϵ^{bulk} = 3.92 eV) projected onto each of the Ag atoms for all the configurations of the two oxidized clusters as a function

of N_B (Fig. 3). The average $\Delta\epsilon_d$ value for each N_B is shown as green square. Remarkably, such behavior follows the evolution of the calculated CLS reported in Fig. 3a and whose average values are also included in the Fig. 3c for comparison. This is a striking difference with respect to the case of Ag single crystal surfaces, where ϵ_d is clearly not affected by N_B [18]. This is a sign that, in the case of clusters, the Ag – O bonds involve also electronic d-states, while for single crystal surfaces the bonding is attributed mainly to s-states. Moreover, in the oxidation of the Ag surface, CLSs and ϵ_d are not interdependent, because of a dominant contribution arising form final-state effects. On the other hand, the observation that for the clusters the two quantities follow a similar trend is indicative of a dominance of initial-state effects in determining the CLSs [47,48], as proven in the case of atomic and molecular adsorbates on solid surfaces [49–51].

To investigate the origin of this result, we analyzed the Ag 4d and O 2p partial density of states (PDOS). In Fig. 4 we report the Ag 4d PDOS of a representative set of atoms in the oxidized clusters for each N_B and the associated O 2p PDOS. Generally, the interaction of O 2p states with the d states of transition metals such as Ru [16], Rh [52] and Pd [18] causes a broadening of the d-band, with the formation of bonding and anti-bonding states close to and above the Fermi level. In particular, the presence of d-states above the Fermi level requires a change in the position of ϵ_d in order to maintain charge neutrality. This adjustment moves the band towards higher BE and the corresponding attractive contribution to the Kohn-Sham potential is reflected in a positive CLS when N_B increases. For the atoms in the Ag$_7$ and Ag$_{11}$ cluster with N_B = 0–2 we observe that the d-band progressively moves towards the Fermi level as N_B increases, but it remains always confined below the Fermi level. Only for N_B = 3 and 4 the Ag d-band crosses the Fermi level, with the anti-bonding states appearing in the range $\epsilon_F - \epsilon$ = 0 ÷ −1 eV. This requires an adjustment of ϵ_d, which moves the d-band towards higher BE. The corresponding attractive contribution to the Kohn-Sham potential is reflected in the inversion of the CLS trend that we observe for N_B = 4 which is pushed towards higher BE causing the CLS anomaly.

It is essential to stress that a change in the oxidation state of the clusters does not automatically yield an effect in the experimental data. Such hin- drance is essentially due to the high Gaussian width of the spectra and to the hybrid structure of the clusters, which contain atoms
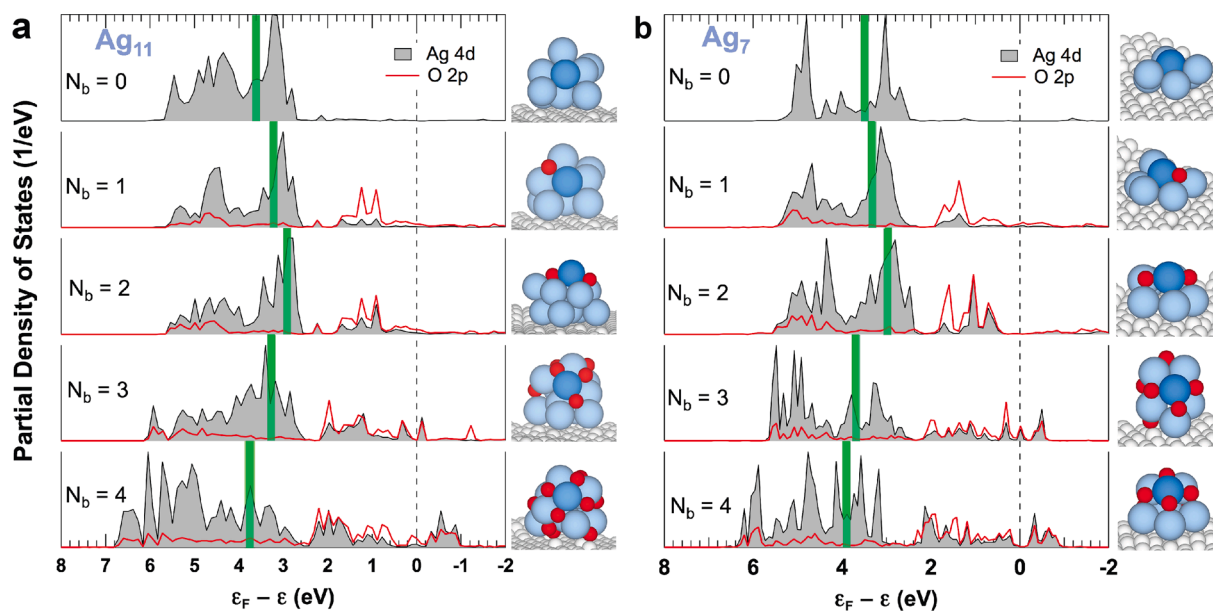

Fig. 4. (a) Ag 4d and O 2p PDOS of atoms composing the Ag$_{11}$ and (b) Ag$_7$ clusters for each N_B in the range N_B = 0–4. On the right-hand side of each plot, we reported ball model of the associated relaxed structures for each N_B. d-band centers, illustrated in Fig. 3(c), are reported as green vertical lines. Grey balls represent C atoms, red balls stand for O, light blue represents Ag. (For interpretation of the references to colour in this figure legend, the reader is referred to the web version of this article.)

with both 1 + and 3 + oxidation state. A consequence of this is that the average CLS (Fig. 5) of the oxidized clusters increases with increasing O:Ag ratio, in agreement with the experimental CLS (Fig. 2a and 2b). As a matter of fact, the lower CLS of Ag(III) ions is counterbalanced by the larger CLS associated to Ag(I) ions, which can still be observed also in the cluster with high-oxygen density. In order to experimentally observe an inversion of the binding energies trend, one should be able to reach such an O density in the cluster that will lead to increase the numbers of Ag atoms with $N_B = 4$ configuration, moving towards the Ag_2O_3 oxide phase. Whereas the latter was not experimentally achieved in our experiment, the trend of the average CLS was instrumental to experimentally find the density of oxygen atoms on the cluster. We have indeed found a O:Ag ratio close to 1 for both clusters, although this is not enough to experimentally show the inversion of the CLS for the 3+ oxidation state.

The changes in the d-band center ϵ_d and the different initial and final state contribution to the total CLS is strongly connected to the quasi-zero dimensional character and low nuclearity of the Ag clusters, since this behavior is not observed for solid surfaces, where ϵ_d remains substantially unaltered by the oxygen coverage and there is no correlation with the number of O-Ag bonds. Shifts of the ϵ_d are of particular interest

because, according to the Hammer-Nørskov model [53], they are generally associated to changes in the chemical reactivity of a system, as also proved in the case of nanoclusters [54]. Recent works discussed possible ways to modify ϵ_d doping a nanomaterial to enhance its catalytic properties [55–58]. For example, it was possible to shift ϵ_d of Ag-based nanoparticles by almost 0.2 eV by doping them with Pd atoms and forming an alloy [59]. According to this well-established rule, the adsorbed O progressively enhances the reactivity of the Ag_7 and Ag_{11} clusters, as the d-band center moves up to 1.0 eV closer to the Fermi level for $N_B = 2$. Moreover, the dominant contribution of the initial state effects to the total CLS allows to follow the ϵ_d shifts, and thus the reactivity changes by means of XPS, thanks to their direct proportionality. The ability to disentangle the initial state contribution to the CLS in metallic clusters has allowed in the past to link their catalytic and electronic properties [41]. Achieving a similar result also in the case of oxidized atomic clusters or, more in general, low nuclearity systems involving oxidized atoms, could help in bridging the gap between the understanding of catalytic reaction dynamics and the atomic level description of their geometric and electronic properties with the final goal of improving the methods for catalyst design [60,61].

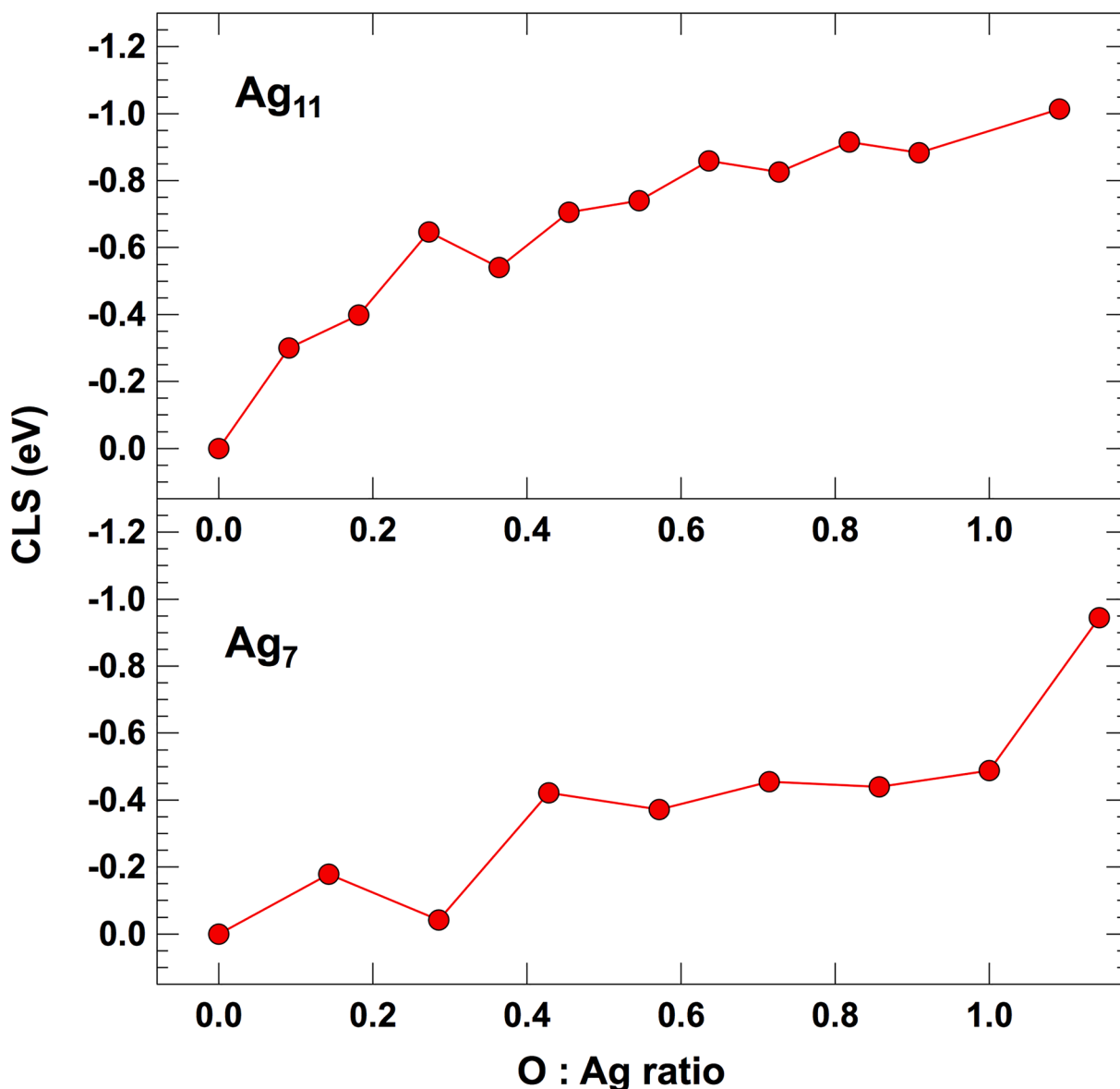Our results show that the well-established trend studied for bulk and

Fig. 5. (a) Average DFT calculated Ag 4d CLS of Ag_{11} and (b) Ag_7 oxidized clusters as a function of the O: Ag ratio.

surface oxides may be different in low-nuclearity oxidized systems. This could have implications, for example, in the study of SiO_2, one of the most important bulk-oxides studied in materials science, which is often considered as a model system to explain the correlation between core-level shifts and oxidation state [62,63]. Since Si has 4 valence electrons, its oxidation number can range from $1+$ to $4+$ when it binds to oxygen.. The core level of Si $2p$ then scales with the oxidation state, with an increase in $2p$ binding energy of approximately 1 eV/oxidation state. Therefore, considering the bulk behavior, it would be very interesting to evaluate the trend of the $2p$ levels of Si in the case of clusters formed by only a few atoms to verify if the anomaly found in our case can be extended also to other nano-oxides.

4. Conclusion

We have shown that core levels of quasi-zero dimensional Ag oxides be- have in a radically different way from the bulk or surface case, given their unique electronic structure. The different behavior of the Ag $3d_{5/2}$ CLS in the low nuclearity clusters compared to Ag surface oxides and ultra-thin films manifests through an anomalous trend when increasing the number of Ag to O bonds. An in-depth analysis of the Ag $4d$-band based on DFT calculation allowed us also to directly link such anomaly to the shift of the d-band center, thus suggesting that CLS are dominated by initial state effects and related to changes in chemical reactivity. In addition, we conclude that moderate O adsorption on Ag_7 and Ag_{11} clusters could enhance their reactivity, with the adsorbents that indirectly interact through the metal d-band. Finally, our results suggest that oxidized size-selected Ag clusters can be taken in consideration as low-nuclearity supported catalysts, also in the form of alloy [64], to maximize the reaction and cost efficiency, as already proved in the case of other single-atoms and subnanometer metallic oxides [65–70], specifically in the case of the epoxidation reaction [71,72], or for biomedical applications [73].

Author contribution

Federico Loi: Formal analysis, Data curation, Investigation, Writing – original draft, Writing – review & editing. **Monica Pozzo:** Formal analysis, Investigation, Writing – review & editing. **Luca Sbuelz:** Investigation, Writing – review & editing. **Luca Bignardi:** Investigation, Writing – review & editing. **Paolo Lacovig:** Investigation, Writing – review & editing. **Ezequiel Tosi:** Investigation, Writing – review & editing. **Silvano Lizzit:** Investigation, Writing – review & editing. **Aras Kartouzian:** Validation, Investigation, Writing – review & editing. **Ulrich Heiz:** Validation, Investigation, Writing – review & editing. **Rosanna Larciprete:** Validation, Investigation, Writing – review & editing. **Dario Alfè:** Formal analysis, Investigation, Investigation, Writing – review & editing. **Alessandro Baraldi:** Conceptualization, Investigation, Supervision, Investigation, Writing – original draft, Writing – review & editing.

Declaration of Competing Interest

The authors declare that they have no known competing financial interests or personal relationships that could have appeared to influence the work reported in this paper.

Data availability

Data will be made available on request.

Acknowledgements

Appendix A. Supplementary material

Supplementary data to this article can be found online at https://doi.org/10.1016/j.apsusc.2023.156755.

References

[1] A. Walsh, A.A. Sokol, J. Buckeridge, D.O. Scanlon, C.R.A. Catlow, Oxidation states and ionicity, Nat. Mater. 17 (11) (2018) 958–964.

[2] I.D. Brown, Recent developments in the methods and applications of the bond valence model, Chem. Rev. 109 (12) (2009) 6858–6919.

[3] N. Daelman, M. Capdevila-Cortada, N. Ĺopez, Dynamic charge and oxidation state of Pt/CeO_2 single-atom catalysts, Nat. Mater. 18 (11) (2019) 1215–1221.

[4] K.M. Jablonka, D. Ongari, S.M. Moosavi, B. Smit, Using collective knowledge to assign oxidation states of metal cations in metal-organic frameworks, Nat. Chem. 13 (8) (2021) 771–777.

[5] K. Siegbahn, D. Hammond, H. Fellner-Feldegg, E. Barnett, Electron spectroscopy with monochromatized x-rays: This technique constitutes a second-generation approach for a new analytical method, Science 176 (4032) (1972) 245–252.

[6] E. Sokolowski, C. Nordling, K. Siegbahn, Chemical shift effect in inner electronic levels of Cu due to oxidation, Phys. Rev. 110 (3) (1958) 776.

[7] J.J. Navarro, M. Das, S. Tosoni, F. Landwehr, J.P. Bruce, M. Heyde, G. Pacchioni, F. Glorius, B.R. Cuenya, Covalent adsorption of N- heterocyclic carbenes on a copper oxide surface, J. Am. Chem. Soc. 144 (36) (2022) 16267–16271.

[8] W. Wang, C. Deng, S. Xie, Y. Li, W. Zhang, H. Sheng, C. Chen, J. Zhao, Photocatalytic c–c coupling from carbon dioxide reduction on copper ox- ide with mixed-valence copper(i)/copper(ii), J. Am. Chem. Soc. 143 (7) (2021) 2984–2993.

[9] M. T. Greiner, T. E. Jones, A. Klyushin, A. Knop-Gericke, R. Schlögl, Ethylene epoxidation at the phase transition of copper oxides, J. Am. Chem. Soc. 139 (34) (2017) 11825–11832.

[10] A. Verdaguer-Casadevall, C.W. Li, T.P. Johansson, S.B. Scott, J.T. McKeown, M. Kumar, I.E.L. Stephens, M.W. Kanan, I. Chorkendorff, Probing the active surface sites for CO reduction on oxide-derived copper electrocatalysts, J. Am. Chem. Soc. 137 (31) (2015) 9808–9811.

[11] F.J. Himpsel, J.F. Morar, F.R. McFeely, R.A. Pollak, G. Hollinger, Core-level shifts and oxidation states of Ta and W: Electron spectroscopy for chemical analysis applied to surfaces, Phys. Rev. B 30 (1984) 7236–7241.

[12] G. Schön, J. Tummavuori, B. Lindström, C. Enzell, C. Enzell, C. Swahn, ESCA studies of Ag, Ag_2O and AgO, Acta Chem. Scand. 27 (7) (1973) 2623.

[13] X. Bao, M. Muhler, T. Schedel-Niedrig, R. Schlögl, Interaction of oxygen with silver at high temperature and atmospheric pressure: A spectroscopic and structural analysis of a strongly bound surface species, Phys. Rev. B 54 (1996) 2249–2262.

[14] T. Kaspar, T. Droubay, S. Chambers, P. Bagus, Spectroscopic evidence for Ag(III) in highly oxidized silver films by X-ray photoelectron spectroscopy, J. Phys. Chem. C 114 (49) (2010) 21562–21571.

[15] A. Baraldi, Structure and chemical reactivity of transition metal surfaces as probed by synchrotron radiation core level photoelectron spectroscopy, J. Phys. Condens. Matter 20 (9) (2008) 093001.

[16] S. Lizzit, A. Baraldi, A. Groso, K. Reuter, M.V. Ganduglia-Pirovano, C. Stampfl, M. Scheffler, M. Stichler, C. Keller, W. Wurth, et al., Surface core-level shifts of clean and oxygen-covered Ru(0001), Phys. Rev. B 63 (20) (2001) 205419.

[17] M.V. Ganduglia-Pirovano, M. Scheffler, A. Baraldi, S. Lizzit, G. Comelli, G. Paolucci, R. Rosei, Oxygen-induced Rh $3d_{5/2}$ surface core-level shifts on Rh (111), Phys. Rev. B 63 (2001), 205415.

[18] H. Grönbeck, S. Klacar, N. M. Martin, A. Hellman, E. Lundgren, J. N. Andersen, Mechanism for reversed photoemission core-level shifts of ox- idized Ag, Phys. Rev. B 85 (11) (2012) 115445.

[19] M. Gajdoš, A. Eichler, J. Hafner, Ab initio density functional study of O on the Ag (001) surface, Surf. Sci. 531 (3) (2003) 272–286.

[20] N. M. Martin, S. Klacar, H. Grönbeck, J. Knudsen, J. Schnadt, S. Blomberg, J. Gustafson, E. Lundgren, High-coverage oxygen-induced surface structures on Ag (111), J. Phys. Chem. C 118 (28) (2014) 15324– 15331.

[21] F. Loi, M. Pozzo, L. Sbuelz, L. Bignardi, P. Lacovig, E. Tosi, S. Lizzit, A. Kartouzian, U. Heiz, D. Alfè, A. Baraldi, Oxidation at the sub- nanoscale: Oxygen adsorption on graphene-supported size-selected Ag clusters, J. Mat. Chem. A 10 (27) (2022) 14594–14603.

[22] D. Alfè, M. Pozzo, E. Miniussi, S. Günther, P. Lacovig, S. Lizzit, R. Lar- ciprete, B. S. Burgos, T. Menteş, A. Locatelli, et al., Fine tuning of graphene-metal adhesion by surface alloying, Sci. Rep. 3 (1) (2013) 1–6.

[23] U. Heiz, F. Vanolli, L. Trento, W.-D. Schneider, Chemical reactivity of size-selected supported clusters: An experimental setup, Rev. Sci. Instrum. 68 (5) (1997) 1986–1994.

[24] L. Sbuelz, F. Loi, M. Pozzo, L. Bignardi, E. Nicolini, P. Lacovig, E. Tosi, S. Lizzit, A. Kartouzian, U. Heiz, et al., Atomic undercoordination in Ag islands on Ru(0001) grown via size-selected cluster deposition: An experimental and theoretical high-

resolution core-level photoemission study, J. Phys. Chem. C 125 (17) (2021) 9556–9563.

[25] C. Binns, Nanoclusters deposited on surfaces, Surf. Sci. Rep. 44 (1–2) (2001) 1–49.

[26] S. Doniach, M. Sunjic, Many-electron singularity in x-ray photoemission and x-ray line spectra from metals, J. Phys. C 3 (2) (1970) 285.

[27] G. Kresse, J. Furthmüller, Efficient iterative schemes for ab-initio total- energy calculations using a plane-wave basis set, Phys. Rev. B 54 (16) (1996) 11169.

[28] P.J. Feibelman, Pinning of graphene to Ir(111) by flat Ir dots, Phys. Rev. B 77 (16) (2008), 165419.

[29] I. Hamada, Van Der Waals density functional made accurate, Phys. Rev. B 89 (12) (2014), 121103.

[30] P. E. Blöchl, Projector augmented-wave method, Phys. Rev. B 50 (24) (1994) 17953.

[31] J.P. Perdew, K. Burke, M. Ernzerhof, Generalized gradient approximation made simple, Phys. Rev. Lett. 77 (18) (1996) 3865.

[32] X. Liu, C.-Z. Wang, M. Hupalo, W. Lu, M.C. Tringides, Y. Yao, K.-M. Ho, Metals on graphene: Correlation between adatom adsorption behavior and growth morphology, Phys. Chem. Chem. Phys. 14 (25) (2012) 9157–9166.

[33] D. Martoccia, P. Willmott, T. Brugger, M. Björck, S. Günther, C. Schlepütz, A. Cervellino, S. Pauli, B. Patterson, S. Marchini, et al., Graphene on Ru(0001): A 25 × 25 supercell, Phys. Rev. Lett. 101 (12) (2008) 126102.

[34] X. Liu, Y. Han, J.W. Evans, A.K. Engstfeld, R.J. Behm, M.C. Tringides, M. Hupalo, H.-Q. Lin, L. Huang, K.-M. Ho, et al., Growth morphology and properties of metals on graphene, Prog. Surf. Sci. 90 (4) (2015) 397–443.

[35] R.T. Frederick, Z. Novotny, F.P. Netzer, G.S. Herman, Z. Dohnalek, Growth and stability of titanium dioxide nanoclusters on graphene/Ru(0001), J. Phys. Chem. B 122 (2) (2018) 640–648.

[36] B. Wang, B. Yoon, M. König, Y. Fukamori, F. Esch, U. Heiz, U. Landman, Size- selected monodisperse nanoclusters on supported graphene: Bonding, isomerism, and mobility, Nano Lett 12 (11) (2012) 5907–5912.

[37] R. Li, X. Xu, B. Zhu, X.-Y. Li, Y. Ning, R. Mu, P. Du, M. Li, H. Wang, J. Liang, et al., In situ identification of the metallic state of Ag nan- oclusters in oxidative dispersion, Nat. Commun. 12 (1) (2021) 1–9.

[38] C. Rajesh, S. Nigam, C. Majumder, The structural and electronic properties of Au$_n$ clusters on the α-Al$_2$O$_3$(0001) surface: a first principles study, Phys. Chem. Chem. Phys. 16 (2014) 26561–26569.

[39] R. Dietsche, D. C. Lim, M. Bubek, I. Lopez-Salido, G. Ganteför, Y. D. Kim, Comparison of electronic structures of mass-selected Ag clusters and thermally grown Ag islands on sputter-damaged graphite surfaces, Appl. Phys. A 90 (3) (2008) 395–398.

[40] M. Al-Hada, L. Gregoratti, M. Amati, M. Neeb, Pristine and oxidised Ag- nanoparticles on free-standing graphene as explored by X-ray photoelectron and Auger spectroscopy, Surf. Sci. 693 (2020), 121533.

[41] W.E. Kaden, T. Wu, W.A. Kunkel, S.L. Anderson, Electronic structure controls reactivity of size-selected Pd clusters adsorbed on TiO$_2$ surfaces, Science 326 (5954) (2009) 826–829.

[42] B.S. Mitchell, A. Chirila, J.A. Kephart, A.C. Boggiano, S.M. Krajewski, D. Rogers, W. Kaminsky, A. Velian, Metal–support interactions in molecular single-site cluster catalysts, J. Am. Chem. Soc. 144 (40) (2022) 18459–18469.

[43] A. Nilsson, N. Mårtensson, Vibrational broadening in core-level spectra from adsorbates: C, N and O on Ni(100), Phys. Rev. Lett. 63 (1989) 1483.

[44] W. Eberhardt, P. Fayet, D.M. Cox, Z. Fu, A. Kaldor, R. Sherwood, D. Sondericker, Photoemission from mass-selected monodispersed Pt clusters, Phys. Rev. Lett. 64 (1990) 780.

[45] Y.S. Kim, A. Bostwick, E. Rotenberg, P.N. Ross, S.C. Hong, B.S. Mun, The study of oxygen molecules on Pt(111) surface with high resolution x-ray photoemission spectroscopy, J. Chem. Phys. 133 (3) (2010), 034501.

[46] R. Bader, Atoms in Molecules: A Quantum Theory, Clarendon Press (Oxford), International series of monographs on chemistry, 1990.

[47] D.G. Pettifor, Bonding and Structure of Molecules and Solids, Clarendon Press (Oxford), 1995.

[48] A. Zangwill, Physics at Surfaces, Cambridge University Press, 1988.

[49] A. Baraldi, S. Lizzit, G. Comelli, M. Kiskinova, R. Rosei, K. Honkala, J.K. Nørskov, Spectroscopic link between adsorption site occupation and local surface chemical reactivity, Phys. Rev. Lett. 93 (2004) 046101.

[50] L. Bianchettin, A. Baraldi, S. de Gironcoli, S. Lizzit, L. Petaccia, E. Vesselli, G. Comelli, R. Rosei, Geometric and electronic structure of the N/Rh(100) system by core-level photoelectron spectroscopy: Experiment and theory, Phys. Rev. B 74 (2006), 045430.

[51] L. Bianchettin, A. Baraldi, E. Vesselli, S. de Gironcoli, S. Lizzit, L. Petaccia, G. Comelli, R. Rosei, Experimental and theoretical surface core level shift study of the S-Rh(100) local environment, J. Phys. Chem. C 111 (10) (2007) 4003–4013.

[52] M.V. Ganduglia-Pirovano, M. Scheffler, Structural and electronic properties of chemisorbed oxygen on Rh(111), Phys. Rev. B 59 (23) (1999) 15533.

[53] B. Hammer, J. Nørskov, Theoretical surface science and catalysis– calculations and concepts, in: Impact of Surface Science on Catalysis, Vol. 45 of Advances in Catalysis, Academic Press, 2000, pp. 71–129.

[54] S. Nigam, C. Majumder, Atomically precise noble metal clusters (Ag$_{10}$, Au$_{10}$, Pd$_{10}$ and Pt$_{10}$) on alumina support: A comprehensive dft study for oxidative catalysis, Appl. Surf. Sci. 547 (2021), 149160.

[55] Y. Cheng, H. Zhang, X. Qu, Electronic band-engineered nanomaterials for biosafety and biomedical application, Acc. Mater. Res. 2 (9) (2021) 764–779.

[56] Y. Zhou, X. Peng, T. Zhang, H. Cai, B. Lin, L. Zheng, X. Wang, L. Jiang, Essential role of Ru–anion interaction in Ru-based ammonia synthesis catalysts, ACS Catal. 12 (13) (2022) 7633–7642.

[57] Y. Zhang, J. Li, J. Cai, L. Yang, T. Zhang, J. Lin, X. Wang, C. Chen, L. Zheng, C.- T. Au, B. Yang, L. Jiang, Construction of spatial effect from atomically dispersed co anchoring on subnanometer Ru cluster for enhanced N$_2$-to-NH$_3$ conversion, ACS Catal. 11 (8) (2021) 4430–4440.

[58] Y. Pan, K. Sun, Y. Lin, X. Cao, Y. Cheng, S. Liu, L. Zeng, W.-C. Cheong, D. Zhao, K. Wu, Z. Liu, Y. Liu, D. Wang, Q. Peng, C. Chen, Y. Li, Electronic structure and d-band center control engineering over M-doped CoP (M=Ni, Mn, Fe) hollow polyhedron frames for boosting hydrogen production, Nano Energy 56 (2019) 411–419.

[59] Y. Chang, Y. Cheng, Y. Feng, K. Li, H. Jian, H. Zhang, Upshift of the D band center toward the fermi level for promoting silver ion release, bacteria inactivation, and wound healing of alloy silver nanoparticles, ACS Appl. Mater. Interfaces 11 (13) (2019) 12224–12231.

[60] S. Mitchell, R. Qin, N. Zheng, J. Pérez-Ramı́rez, Nanoscale engineering of catalytic materials for sustainable technologies, Nat. Nanotechnol. 16 (2) (2021) 129–139.

[61] J. Jašík, A. Fortunelli, Š. Vajda, Exploring the materials space in the smallest particle size range: From heterogeneous catalysis to electro- catalysis and photocatalysis, Phys. Chem. Chem. Phys. 24 (20) (2022) 12083–12115.

[62] F. Himpsel, F. McFeely, A. Taleb-Ibrahimi, J. Yarmoff, G. Hollinger, Microscopic structure of the SiO$_2$/Si interface, Phys. Rev. B 38 (9) (1988) 6084.

[63] A. Pasquarello, M.S. Hybertsen, R. Car, Si 2p core-level shifts at the Si(001)-SiO$_2$ interface: A first-principles study, Phys. Rev. Lett. 74 (6) (1995) 1024.

[64] F. R. Negreiros, A. Halder, C. Yin, A. Singh, G. Barcaro, L. Se- menta, E. C. Tyo, M. J. Pellin, S. Bartling, K.-H. Meiwes-Broer, S. Seifert, P. Sen, S. Nigam, C. Majumder, N. Fukui, H. Yasumatsu, S. Vajda, A. Fortunelli, Bimetallic Ag-Pt sub-nanometer supported clusters as highly efficient and robust oxidation catalysts, Angewandte Chemie International Edition 57 (5) (2018) 1209–1213. arXiv:https:// onlinelibrary.wiley.com/doi/pdf/10.1002/anie.201709784.

[65] E.C. Tyo, S. Vajda, Catalysis by clusters with precise numbers of atoms, Nat. Nanotechnol. 10 (7) (2015) 577–588.

[66] L. DeRita, J. Resasco, S. Dai, A. Boubnov, H.V. Thang, A.S. Hoffman, I. Ro, G. W. Graham, S.R. Bare, G. Pacchioni, et al., Structural evolution of atomically dispersed Pt catalysts dictates reactivity, Nat. Mater. 18 (7) (2019) 746–751.

[67] Z. Li, S. Ji, Y. Liu, X. Cao, S. Tian, Y. Chen, Z. Niu, Y. Li, Well- defined materials for heterogeneous catalysis: From nanoparticles to isolated single-atom sites, Chem. Rev. 120 (2) (2019) 623–682.

[68] M. Lamoth, M. Plodinec, L. Scharfenberg, S. Wrabetz, F. Girgsdies, T. Jones, F. Rosowski, R. Horn, R. Schlögl, E. Frei, Supported Ag nanoparticles and clusters for CO oxidation: Size effects and influence of the silver–oxygen interactions, ACS Appl. Nano Mater. 2 (5) (2019) 2909–2920.

[69] M. Lamoth, T. Jones, M. Plodinec, A. Machoke, S. Wrabetz, M. Krämer, A. Karpov, F. Rosowski, S. Piccinin, R. Schlögl, E. Frei, Nanocatalysts unravel the selective state of Ag, ChemCatChem 12 (11) (2020) 2977– 2988.

[70] K.-G. Liu, X.-M. Gao, T. Liu, M.-L. Hu, D.-E. Jiang, All-carboxylate- protected superatomic silver nanocluster with an unprecedented rhombohedral Ag$_8$ core, J. Am. Chem. Soc. 142 (40) (2020) 16905–16909.

[71] D. Chen, P.-L. Kang, Z.-P. Liu, Active site of catalytic ethene epoxidation: Machine-learning global pathway sampling rules out the metal sites, ACS Catal. 11 (13) (2021) 8317–8326.

[72] T. Pu, A. Setiawan, B.M. Lis, M. Zhu, M.E. Ford, S. Rangarajan, I.E. Wachs, Nature and reactivity of oxygen species on/in silver catalysts during ethylene oxidation, ACS Catal. 12 (8) (2022) 4375–4381.

[73] Y. Fan, S. Liu, Y. Yi, H. Rong, J. Zhang, Catalytic nanomaterials to- ward atomic levels for biomedical applications: From metal clusters to single-atom catalysts, ACS Nano 15 (2) (2021) 2005–2037.